Monthly Notices of the ROYAL ASTRONOMICAL SOCIETY

MNRAS **441,** 442–451 (2014)
Advance Access publication 2014 April 22

doi:10.1093/mnras/stu450

The 55 Cancri planetary system: fully self-consistent *N*-body constraints and a dynamical analysis

Benjamin E. Nelson,[1,2,3]★ Eric B. Ford,[1,2,3] Jason T. Wright,[1,2] Debra A. Fischer,[4] Kaspar von Braun,[5] Andrew W. Howard,[6] Matthew J. Payne[3,7] and Saleh Dindar[8]

[1]*Center for Exoplanets and Habitable Worlds, The Pennsylvania State University, 525 Davey Laboratory, University Park, PA 16802, USA*
[2]*Department of Astronomy and Astrophysics, The Pennsylvania State University, 525 Davey Laboratory, University Park, PA 16802, USA*
[3]*Department of Astronomy, University of Florida, 211 Bryant Space Science Center, Gainesville, FL 32611, USA*
[4]*Department of Astronomy, Yale University, New Haven, CT 06520 USA*
[5]*Max-Planck Institute for Astronomy (MPIA), Königstuhl 17, D-69117 Heidelberg, Germany*
[6]*Institute for Astronomy, University of Hawaii, 2680 Woodlawn Drive, Honolulu, HI 96822, USA*
[7]*Harvard–Smithsonian Center for Astrophysics, 60 Garden Street, Cambridge, MA 02138, USA*
[8]*Department of Computer & Information Science & Engineering, University of Florida, CSE Building, Gainesville, FL 32611, USA*

Accepted 2014 March 4. Received 2014 February 24; in original form 2014 January 4

ABSTRACT

We present an updated study of the planets known to orbit 55 Cancri A using 1 418 high-precision radial velocity observations from four observatories (Lick, Keck, Hobby-Eberly Telescope, Harlan J. Smith Telescope) and transit time/durations for the inner-most planet, 55 Cancri 'e' (Winn et al. 2011). We provide the first posterior sample for the masses and orbital parameters based on self-consistent *N*-body orbital solutions for the 55 Cancri planets, all of which are dynamically stable (for at least 10^8 yr). We apply a GPU version of Radial velocity Using *N*-body Differential evolution Markov Chain Monte Carlo (RUN DMC; Nelson, Ford & Payne) to perform a Bayesian analysis of the radial velocity and transit observations. Each of the planets in this remarkable system has unique characteristics. Our investigation of high-cadence radial velocities and priors based on space-based photometry yields an updated mass estimate for planet 'e' ($8.09 \pm 0.26\ M_\oplus$), which affects its density ($5.51 \pm^{1.32}_{1.00}\ \mathrm{g\,cm^{-3}}$) and inferred bulk composition. Dynamical stability dictates that the orbital plane of planet 'e' must be aligned to within 60° of the orbital plane of the outer planets (which we assume to be coplanar). The mutual interactions between the planets 'b' and 'c' may develop an apsidal lock about 180°. We find 36–45 per cent of all our model systems librate about the anti-aligned configuration with an amplitude of $51^\circ \pm^{6^\circ}_{10^\circ}$. Other cases showed short-term perturbations in the libration of $\varpi_\mathrm{b} - \varpi_\mathrm{c}$, circulation, and nodding, but we find the planets are not in a 3:1 mean-motion resonance. A revised orbital period and eccentricity for planet 'd' pushes it further towards the closest known Jupiter analogue in the exoplanet population.

Key words: methods: statistical – techniques: radial velocities – planets and satellites: dynamical evolution and stability.

1 INTRODUCTION

With roots in early Doppler surveys, 55 Cancri is a wide visual binary system harbouring five known planets with a large range of orbital periods (∼0.7 d to ∼14 yr) and masses (∼$8 M_\oplus$ to ∼$4 M_\mathrm{J}$). The known planets orbit 55 Cancri A, a K0-type dwarf (von Braun et al. 2011), which is also orbited by an M-dwarf at a projected separation of ∼1065 au (Mugrauer et al. 2006). The system has an extensive radial velocity (RV) history using several ground-based facilities (e.g. Lick, Keck, Hobby-Eberly Telescope, Harlan J. Smith Telescope) as well as space-based observatories to constrain properties of the innermost planet. The first eight years of RV measurements from the Lick Observatory showed a strong periodic signal with a period of 14.6 d indicative of an ∼0.8 M_J mass planet named 55 Cancri b (Butler et al. 1997). The RV time series showed other trends due to the presence of two additional massive bodies, 55 Cancri 'c' and 'd' with orbital periods 44.3 and 5360 d, respectively, which were eventually uncovered via additional RV measurements (Marcy et al. 2002). They found the difference between a Keplerian and self-consistent Newtonian fit for a three-planet model is measurable on the observing time-scale, demonstrating that the Keplerian model

★ E-mail: benelson@psu.edu

is insufficient for fitting future observations. RV observations with the Hobby-Eberly Telescope (HET) uncovered a 2.8 d signal of an $\sim$17 $M_\oplus$ planet, initially labelled as 'e' (McArthur et al. 2004). However, in 2010, a re-analysis of these data showed that the previously published orbital period of planet 'e' was an alias and the more likely period was 0.7365 d (Dawson & Fabrycky 2010). The revised ephemeris pushed the mass of 'e' towards the super-Earth regime and raised its transit probability to $\sim$25 per cent. Space-based searches with *MOST* (Winn et al. 2011) and warm *Spitzer* (Demory et al. 2011) showed that planet 'e' did indeed transit. More photometric measurements have refined the planet-to-star radius ratio estimate (Demory et al. 2012; Gillon et al. 2012; Dragomir et al. 2013). A fifth planet 'f' was found with an orbital period of 260 d (Fischer et al. 2008). Additional RVs provided a new mass estimate of planet 'e' and an updated model for the planetary system assuming no planet interactions (Endl et al. 2012).

The complexity of the 55 Cancri system provides valuable information for theoretical investigations, improving our understanding of planetary migration, orbital evolution, and composition. The near 3:1 period commensurability of planets 'b' and 'c' is thought to provide evidence for the planets migrating to their present locations, rather than forming in situ (Kley, Peitz & Bryden 2004). The orbital evolution of this planet pair has been a longstanding problem, especially in the presence of additional planets. It was thought that the three resonant arguments for planets 'b' and 'c' librated, suggesting that they orbited in a mean-motion resonance (Ji et al. 2003; Zhou et al. 2004; Barnes & Greenberg 2007). With additional RV information, the resonant arguments were found to be circulating (Fischer et al. 2008) for the single self-consistent dynamical fit, suggesting they were not in resonance. Injecting a hypothetical sixth planet based on the aforementioned model did not cause libration of these angles (Raymond, Barnes & Gorelick 2008). The binary companion may play a significant role in the long-term orbital evolution of the system. Its gravitational perturbations paired with the rapid planet–planet interactions causes the orbits of the outer-four known planets to precess like a rigid body, so they are likely misaligned with the stellar spin axis of 55 Cancri A (Kaib, Raymond & Duncan 2011). Improved stellar parameters (von Braun et al. 2011) and aforementioned photometric radius estimates for planet 'e' inspired interior composition models that allow us to learn about a planet that is unlike anything in our own Solar system. One noteworthy analysis suggests that 'e' is a solid, carbon-rich planet (Madhusudhan, Lee & Mousis 2012), a chemical composition much different than that of Earth. However, thorough chemical composition models can only be done with extremely precise measurements of the star's radius, C/O ratio, planetary mass, etc. (Teske et al. 2013). The combination of tidal forces and secular interactions with the outer planets are predicted to drive planet 'e' into a state where its eccentricity oscillates with amplitudes ranging from 10^{-4} to 0.17, depending on the orbital parameters and tidal dissipation efficiency (Bolmont et al. 2013). The system as a whole has inspired tests of classical secular theory, which provides insight to the dynamical histories (Laerhoven & Greenberg 2012).

Characterizing the key physical quantities of this landmark exoplanet system requires a combination of these high-precision measurements (both photometric and spectroscopic) and robust physical and statistical modelling. Due to limitations in computational power, aforementioned analyses of the RV data assumed each planet travels on an independent Keplerian orbit. Motivated from the findings of Marcy et al. (2002), Fischer et al. (2008) did report a best-fitting Newtonian model using the period alias for 'e' but not a detailed analysis of parameter uncertainties with a fully self-consistent dynamical model. A generalized *N*-body Markov chain Monte Carlo algorithm applied to RV observations was developed by Nelson et al. (2014) to explore complex χ^2 surfaces in high-dimensional parameter spaces. The 55 Cancri system is a challenging problem due to the length of the RV observing baseline, the sheer number of model parameters, the observed mutual interactions amongst planets, and the short inner orbital period.

In this paper, we present new RVs from the Keck High Resolution Echelle Spectrometer (HIRES), revised constraints on the orbital parameters of the 55 Cancri planets based on a self-consistent dynamical model, and an analysis of the orbital evolution of the system. In Section 2, we describe the Doppler observations used, including a new set made with the Keck HIRES. In Section 3, we briefly describe the RUN DMC algorithm, the parameter space, and our methods for modelling the observations. In Section 4, we present results for each of the 55 Cancri planets. We conclude with a discussion of the key results and the applications of our posterior samples in Section 5.

2 OBSERVATIONS

2.1 Lick, HET, and HJST data

Our investigation of 55 Cancri began as a performance test of RUN DMC using the published 70 Keck and 250 Lick RVs from Fischer et al. (2008) without considering the innermost planet (Nelson et al. 2014). We found that RUN DMC could successfully navigate such a high-dimensional parameter space ($\sim$5 $\times$ number of planets), so it appeared plausible to perform a much more thorough analysis with all five planets, all published RVs, a dynamical model, and a detailed model of the systematics. Next, we included the remaining public RVs, specifically from the HET (McArthur et al. 2004). Endl et al. (2012) eventually announced new McDonald Observatory RVs, including a new Doppler reduction of the McArthur et al. (2004) RVs totalling 131 measurements, and a new set of 212 RVs from the Harlan J. Smith Telescope (HJST). After the RV programme on the Lick observatory's Hamilton spectrograph effectively ended (due to the heater of the iodine cell malfunctioning), Fischer, Marcy & Spronck (2014) released 582 unbinned RV measurements of 55 Cancri. These data include a new reduction of the older RVs as well as new observations. Our final analysis considers RVs from Endl et al. (2012) and Fischer et al. (2014) RVs, as well as new, unbinned HIRES RVs, to be discussed in the subsequent subsection. We will describe the treatment of all these observations in Section 3.2.

2.2 Keck data

Our analysis includes 493 unbinned velocities from Keck HIRES. These RVs consist of a combination of post-Fischer et al. (2008) measurements and individual RVs that were previously reported as one binned measurement. We present Keck observations in Table 1.

We measured relative RVs of 55 Cancri A with the HIRES echelle spectrometer (Vogt et al. 1994) on the 10-m Keck I telescope using standard procedures. Most observations were made with the B5 decker (3.5 $\times$ 0.86 arcsec). Light from the telescope passed through a glass cell of molecular iodine cell heated to 50° C. The dense set of molecular absorption lines imprinted on the stellar spectra in 5000–6200 Å provide a robust wavelength scale against which Doppler shifts are measured, as well as strong constraints on the instrumental profile at the time of each observation (Marcy & Butler 1992; Valenti, Butler & Marcy 1995). We also obtained five iodine-free template spectra using the B1 decker (3.5 $\times$ 0.57 arcsec). These

Table 1. New, unbinned HIRES velocities for 55 Cancri.

BJD−244 0000 (d)	Radial velocity ($m\,s^{-1}$)	Uncertainty ($m\,s^{-1}$)	Offset index
122 19.138 044	−147.87	1.10	0
122 36.014 734	−65.34	1.21	0
122 43.050 683	−58.78	1.17	0
123 07.849 907	−111.75	1.33	0
123 33.997 674	−142.98	1.49	0

Notes. Table 1 is presented in its entirety as Supporting Information with the online version of the article. This stub table is shown for guidance regarding its form and content.

spectra were de-convolved using the instrumental profile measured from spectra of rapidly rotating B stars observed immediately before and after. We measured high-precision relative RVs using a forward model where the de-convolved stellar spectrum is Doppler shifted, multiplied by the normalized high-resolution iodine transmission spectrum, convolved with an instrumental profile, and matched to the observed spectra using a Levenberg–Marquardt algorithm that minimizes the χ^2 statistic (Butler et al. 1996). In this algorithm, the RV is varied (along with nuisance parameters describing the wavelength scale and instrumental profile) until the χ^2 minimum is reached. Each RV uncertainty is the standard error on the mean RV of ∼700 spectral chunks that are separately Doppler analysed. These uncertainty estimates do not account for potential systematic Doppler shifts from instrumental or stellar effects.

3 METHODS

The Radial velocity Using *N*-body Differential evolution Markov Chain Monte Carlo code (RUN DMC; Nelson et al. 2014) was developed to characterize masses and orbits of complex planetary systems with many model parameters. This algorithm specializes in analysing RV time series and extracting the orbital parameters assuming an *N*-body model. The 'differential evolution' aspect (ter Braak 2006) helps accelerate the burn-in phase and the mixing of the parameters, especially when covariant structure is present amongst model parameters. The 55 Cancri system is also ideal for testing the robustness of RUN DMC for a few reasons: (1) there are many RV observations of 55 Cancri spanning a baseline of ∼23 yr; (2) this five-planet system requires a minimum of 25 model parameters, excluding on-sky inclination, RV offsets, and jitters; and (3) the dynamical interactions between 'b' and 'c' are not negligible on the observing time-scale (i.e. not Keplerian).

We developed a version of RUN DMC that utilizes SWARM-NG to perform *N*-body integrations using nVidia graphics cards and the CUDA programming environment (Dindar et al. 2013). This allowed us to more effectively parallelize the evolution of many Markov chains on the microprocessors. On average, the GPU provided a 4–5x speed up over our CPU version. However, the burn-in phase for some individual test runs exceeded the maximum wall-time of 500 h allowed at the University of Florida High Performance Computing Center (UF HPC). Our solution was to simply restart such runs from where they stopped until the target distribution was reached. Still, the generational lag of the autocorrelation was lengthy (∼few thousand) and took on the order of a couple weeks on a GPU to obtain a set of 10 000 effectively independent samples (Nelson et al. 2014). With these posterior samples, we explore the orbital evolution and long-term stability of the system using the hybrid integrator of MERCURY (Chambers 1999). This is the first application of our GPU-based RUN DMC (Dindar et al. 2013).

There are a number of input parameters for RUN DMC. We considered the lessons from Nelson et al. (2014) in order to approach this problem in the most efficient manner. Extrapolating those results to a five-planet system with non-negligible self-interactions, we set $n_{\rm chains} = 256$, $\sigma_\gamma = 0.05$, and MassScaleFactor = 1.0. To accommodate the innermost planet's 0.7365 d orbital period, we set our integration timestep to ∼5 min (Kokubo, Yoshinaga & Makino 1998). We do not consider the wide binary companion, since its perturbations are only significant over very large time-scales.

We generated a Keplerian set of initial conditions using a standard random-walk proposal, Metropolis–Hastings MCMC (Ford 2006). We fed these states into RUN DMC, which ran for more than 100 000 generations (equivalent to over 25 600 000 model evaluations). We utilize the resources of the UF HPC for both our CPU- and GPU-based computations. As mentioned in Section 2.1, we began this analysis only considering the Fischer et al. (2008) RVs from Lick and Keck. As we introduced new data sets, we were required to add new parameters describing instrumental properties (i.e. RV offsets and jitters). We used posterior samples from the previous pilot runs as the initial conditions for parameters shared between both models and synthetically generated initial conditions for every new parameter. In other words, this study began in a lower dimensional parameter space (∼30) that was eased into a higher dimensional parameter space (∼40) including additional RV data and a more detailed instrumental model (to be discussed in Section 3.2).

3.1 Model parameters

We employ RUN DMC to constrain the Keplerian orbital elements of the 55 Cancri system and the instrumental parameters. We characterize the system model with the star mass ($M_\star$) and radius ($R_\star$), plus each planet's mass (m), semimajor axis (a), eccentricity (e), inclination (i), the longitude of periastron (ω), the longitude of ascending node (Ω), and mean anomaly (M) at our chosen epoch (first Lick observation) for each planet, plus the RV zero-point offsets (C), and jitters ($\sigma_{\rm jit}$) for each observatory. We report the orbital periods (P) based on Kepler's Third Law and each body's m and a based in a Jacobi coordinate system.

The 55 Cancri system is well approximated by a coplanar system, i.e. $\Omega = 0$ and i is the same for all planets. Typically, radial velocities do not place strong constraints on i and Ω unless the self-interactions amongst the planets are very strong [e.g. GJ 876 (Rivera et al. 2010); HD82943 (Tan et al. 2013)]. The near 3:1 MMR in 55 Cancri is significant enough to require an *N*-body model but we will show it does not provide a strong constraint on orbital inclination of the planets. However, photometric observations of e's transit from *MOST* place a tight constraint on the inclination of this planet. Thus, we constrain the central transit time, transit duration, and ingress

duration based on measurements reported in Winn et al. (2011). Initially, we assume all orbits are coplanar. In our final analysis, we allow 'e' to have a different i and Ω than the outer four planets, but assume the outer planets are coplanar with each other.

Because the estimates of the orbital parameters of 'e' now depend on the photometry and thus the radius of the star $R_\star$, we adopt the interferometric measurement of $R_\star$ reported by von Braun et al. (2011). Since we are performing N-body integrations to compute the induced RV signal, our initial conditions must specify the mass of each body. The uncertainty in stellar radius propagates to the stellar mass and further to planet masses. We consider how $M_\star$ changes with $R_\star$ at a constant effective temperature, $T_{\rm eff}$, from spectroscopy. Starting with the mass–luminosity relation $L_\star \sim M_\star^y \sim T_{\rm eff}^4 R_\star^2$, we can derive

$$\left.\frac{\partial M_\star}{\partial R_\star}\right|_{T_{\rm eff}} \sim \frac{2}{y}\frac{M_\star}{R_\star}. \quad (1)$$

Using theoretical stellar models, we solved for y by adopting the observed $T_{\rm eff}$ =5196 K and $L_\star = 0.582\,{\rm L}_\odot$ from von Braun et al. (2011). We generated Y^2 isochrones (Demarque et al. 2004) and found the best y value for multiple ages: 4.125 (8 Gyr), 4.602 (9 Gyr), 5.15 (10 Gyr), 5.491 (11 Gyr), and 5.817 (12 Gyr). For this analysis, we adopted $y = 5.15$ since it corresponds with the age estimate for 55 Cancri (von Braun et al. 2011). Despite such a relatively steep power law, subsequent test runs showed that our conclusions were not sensitive to whether we allowed for uncertainty in $M_\star$ described above or assumed a fixed $M_\star$ value.

3.2 Model of observations

Based on preliminary tests, we generalized RUN DMC to allow for three complications which were not considered in previous analyses.

First, we divided the Fischer et al. (2008) Lick data set into three subsets based on which CCD Dewar was used for each observation. We found that different Dewars used on the Lick Hamilton spectrograph do not give consistent RV zero-point offsets (Wright, private communication), consistent with results from Fischer et al. (2014). Therefore, we adopt a different velocity offset depending on which Dewar was being used at the time. With the Fischer et al. (2014) velocities, the offsets were determined by the Dewar codes: 6, 8, 39, 18, and 24. Dewar code '6' has five observations ranging from JD−244 0000 = 7578.7300 to 8375.6692 ($C_{1,\rm Lick}$). Dewar code '8' has 12 observations ranging from JD−244 0000 = 8646.0011 to 9469.6478 ($C_{2,\rm Lick}$). These early Doppler era observations are expected to have relatively high jitter values. Dewar code '39' (Dewar 13 in actuality) has 96 observations ranging from JD−244 0000 = 9676.0632 to 112 98.722 ($C_{3,\rm Lick}$). Dewar code '18' (Dewar 6 in actuality) has 91 observations ranging from JD−244 0000 = 111 53.033 to 124 09.739 ($C_{4,\rm Lick}$). Dewar code '24' (Dewar 8 in actuality) has 378 observations ranging from JD−244 0000 = 122 67.957 to 156 03.809 ($C_{5,\rm Lick}$) and overlaps with the time series from Dewar code '18'. Particle events may have increased the jitter for the latter (Wright, private communication).

Similarly, we split the Keck data set based on whether observations were taken before or after the CCD upgrade and new Doppler reduction process in 2004. These two subsets received separate velocity zero-point offset parameters. Specifically, the pre-CCD upgrade era has 24 observations ranging from BJD−244 0000 = 122 19.138 044 to 13 077.041 736 ($C_{1,\rm Keck}$). The post-CCD upgrade era has 469 observations ranging from BJD−244 0000=133 39.043 299 to 157 28.743 727 ($C_{2,\rm Keck}$). We also consider HJST and reanalysed HET observations provided by Endl et al. (2012). Each of these data sets has its own offset ($C_{\rm HET}$ and $C_{\rm HJST}$) relative to the large RV zero-points reported by Endl et al. (2012). In total, we model nine RV offsets.

Secondly, we include multiple jitter parameters, $\sigma_{\rm jit}$, one for each observatory. Jitter models scatter in observations beyond what is expected from the formal measurement uncertainties. Jitter may be due to astrophysical noise (e.g. p-modes or chromospheric activity on the star) and/or unmodelled instrumental effects. We performed preliminary analyses using various combinations of our four data sets (e.g. Keck only, Keck+HET, Keck+Lick, Keck+HET+Lick, etc.). We found that introducing the Lick data set increased our jitter estimate. Furthermore, we expect that $\sigma_{\rm jit}$ varied within the Lick time series itself (Fischer et al. 2014). Therefore, we define three Lick jitter terms for Dewar codes 6 and 8 ($\sigma_{\rm jit,Lick1}$), 39 and 18 ($\sigma_{\rm jit,Lick2}$), and 24 ($\sigma_{\rm jit,Lick3}$). We also assign a jitter for Keck ($\sigma_{\rm jit,Keck}$), HET ($\sigma_{\rm jit,HET}$), and HJST ($\sigma_{\rm jit,HJST}$), totalling six jitter terms. For each observation, we substitute the appropriate jitter term for $\sigma_{\rm jit}$ in our likelihood function (equations 4 and 5 in Nelson et al. 2014). We modified our likelihood function to include both RV observations and light-curve parameters measured from the transit light-curve observations for planet 'e'. Our $\chi^2_{\rm eff}$ from Nelson et al. (2014) is adjusted as such:

$$\chi^2_{\rm eff} = \chi^2 + \sum_k \ln\left[\frac{\sigma_{\star,\rm obs}(t_k,\, j_k)^2 + \sigma_{\rm jit}^2}{\sigma_{\star,\rm obs}(t_k,\, j_k)^2}\right] + \sum_{{\rm TT},d_{\rm t},d_{\rm in},R_\star} \frac{(X - X_{\rm obs})^2}{\sigma_X^2} \quad (2)$$

where TT, $d_{\rm t}$, $d_{\rm in}$, and $R_\star$ are the transit time, transit duration, ingress duration, and stellar radius, respectively. From Winn et al. (2011), we use TT = 245 5607.055 62 ± 0.000 87 HJD, $d_{\rm t} = 0.0658 \pm 0.0013$d, and $d_{\rm in} = 0.001\,34 \pm 0.000\,11$d. From von Braun et al. (2011), we use $R_\star = 0.943 \pm 0.010\,{\rm R}_\odot$.

Lastly, we considered possible correlations amongst multiple RV observations. In our standard RUN DMC, the model of observations assumes the RV measurement errors are normally distributed and uncorrelated with one another. This is usually an excellent approximation when observations are separated by one or more days. For bright stars like 55 Cancri, the required exposure time is often less than a minute, which is not long enough to average over solar-like p-mode oscillations. In the past when multiple RV observations were taken sequentially, observers binned these observations and reported a single measurement in an attempt to average over the stellar noise and improve the RV precision. The resulting coarse time series makes it difficult to probe orbital periods in the sub-day regime. However, 55 Cancri A is a very bright RV target (V∼6), and observations can be binned more frequently (every ∼10 min) with enough dedicated telescope time. Unfortunately, this introduces the potential for significant correlations amongst back-to-back observations. Rather than trying to model these correlations in detail, we consider two extreme cases: (1) the typical assumption that all RV errors are uncorrelated (hereafter Case 1) and (2) the measurement errors of observations taken within a maximum of 10 min from each other are perfectly correlated (hereafter Case 2). To simulate the latter, we scale the uncertainties of back-to-back RVs by the square root of the number of observations in that set. For example, the RV uncertainties in each of a set of 12 short-cadence observations are scaled up by $\sqrt{12} = 3.464$. In reality, the true correlation amongst RV observations is somewhere in between these two extreme assumptions. As we will show, the differences in the values for the majority of model parameters were negligible. Table 2 provides a convenient reference for the definitions of Cases 1 and 2, as these

Table 2. Definitions for Cases 1 and 2. In choosing a set of models for subsequent analyses, we recommend using Case 2.

Term	Definition
Case 1	All observation errors as uncorrelated
Case 2	Errors of 'back-to-back' observations are perfectly correlated

Notes. Further details are addressed in Section 3.2.

terms will be used throughout the rest of the paper. We perform two sets of RUN DMC jobs based on Cases 1 and 2.

4 RESULTS

We apply the RUN DMC algorithm to 1418 RV observations spanning an observing baseline of ∼23 yr. We obtain $\chi^2 = 1419 \pm 52$ and $\chi^2 = 1333 \pm 49$ for Cases 1 and 2, respectively. Table 3 lists our estimations of all the planetary parameters for both cases. Our estimates for the zero-point offsets and jitters are shown in Table 4.

We estimate the RV residuals by averaging the orbital elements in our RUN DMC ensemble for the last Markov chain generation and subtract the RV curve predicted by the *N*-body mode from our RV data. The effective residual uncertainties are based on adding the root-mean-square (rms) RV residuals and measurement uncertainties in quadrature. In Fig. 1, we plot the residual periodograms for Cases 1 and 2. We find no obviously significant signals. There are significant peaks in regions associated with common time sampling aliases, e.g. near one-day and one-year, but a peak near 60.7589 d stands out in both cases. It is not immediately obvious whether a planet at this orbital period would be prone to instabilities due to the proximity of planets 'b', 'c', and 'f'. We use a Keplerian MCMC (Ford 2006) to fit the residual RVs with a one-planet model at the 60.7589 d peak. The posterior distribution is multi-modal, the median eccentricity is large (∼0.5), and the half-amplitude is ∼2 m s^{-1}, less than any of our $\sigma_{\rm jit}$ estimates. We note that Baluev (2013) presented a highly parallelized Fourier decomposition algorithm that analysed the Fischer et al. (2008) velocities and uncovered a 9.8 d signal. We do not detect such a signal in our extended data set.

The following subsections describe our results for each of the known 55 Cancri planets and the orbital dynamics of the system. Our results are based on posterior samples from the Markov chain output of RUN DMC and these are fed into MERCURY as sets of initial conditions for the dynamical simulations.

4.1 The transiting planet, 55 Cancri e

The high cadence of the RV time series provides excellent sampling of orbital periods, even those less than one day like planet 'e'. We find the biggest difference between Case 1 and Case 2 is seen in planet e's velocity amplitude, $K_{\rm e}$ (6.04 ± 0.19 and 6.12 ± 0.20 m s^{-1}) and therefore $m_{\rm e}$. When assuming Case 2, the median values of $K_{\rm e}$ and $m_{\rm e}$ shift to greater values relative to Case 1, compensating for the reduced RV information. For $e_{\rm e}$, both cases are consistent with zero. Given the age of the star and the typical time-scales for tidal circularization, one would expect $e_{\rm e} \sim 0$, but

Table 3. Orbital parameter estimates for all the known 55 Cancri planets from self-consistent dynamical fits.

Parameter	Planet e	Planet b	Planet c	Planet f	Planet d
P (d)	$0.736\,5478^{+0.000\,0014}_{-0.000\,0011}$ $0.736\,5478^{+0.000\,0016}_{-0.000\,0012}$	$14.652\,76^{+0.000\,82}_{-0.000\,89}$ $14.653\,14^{+0.000\,90}_{-0.000\,95}$	$44.380^{+0.020}_{-0.018}$ $44.373^{+0.020}_{-0.018}$	261.04 ± 0.37 260.91 ± 0.36	4872^{+28}_{-24} 4867^{+25}_{-26}
$P_{\rm avg}$ (d)	$0.736\,550\,15^{+0.000\,000\,93}_{-0.000\,002\,12}$ $0.736\,550\,12^{+0.000\,000\,99}_{-0.000\,001\,77}$	$14.651\,248^{+0.000\,084}_{-0.000\,088}$ $14.651\,248^{+0.000\,087}_{-0.000\,094}$	$44.4120^{+0.0050}_{-0.0052}$ 44.4094 ± 0.0055	261.04 ± 0.37 260.91 ± 0.36	4872^{+28}_{-24} 4867^{+25}_{-26}
K (m s^{-1})	6.04 ± 0.19 6.12 ± 0.20	$71.60^{+0.19}_{-0.21}$ 71.47 ± 0.21	$10.46^{+0.18}_{-0.19}$ 10.48 ± 0.21	4.75 ± 0.19 4.80 ± 0.20	$47.03^{+0.40}_{-0.41}$ $47.30^{+0.44}_{-0.41}$
m ($M_{\rm J}$)	$0.025\,13 \pm 0.000\,79$ $0.025\,47^{+0.000\,82}_{-0.000\,81}$	$0.844^{+0.124}_{-0.034}$ $0.840^{+0.131}_{-0.031}$	$0.1783^{+0.0261}_{-0.0078}$ $0.1784^{+0.0275}_{-0.0078}$	$0.1475^{+0.0207}_{-0.0093}$ $0.1479^{+0.0219}_{-0.0093}$	$3.83^{+0.57}_{-0.15}$ $3.86^{+0.60}_{-0.15}$
a (au)	$0.015\,439 \pm 0.000\,015$ $0.015\,439 \pm 0.000\,015$	$0.113\,39 \pm 0.000\,11$ $0.113\,39 \pm 0.000\,11$	$0.237\,38 \pm 0.000\,24$ $0.237\,35 \pm 0.000\,24$	0.7735 ± 0.0010 0.7733 ± 0.0010	$5.451^{+0.021}_{-0.019}$ 5.446 ± 0.020
e	$0.034^{+0.022}_{-0.021}$ $0.028^{+0.022}_{-0.019}$	$0.0023^{+0.0025}_{-0.0016}$ $0.0023^{+0.0025}_{-0.0016}$	$0.073^{+0.013}_{-0.014}$ $0.072^{+0.013}_{-0.014}$	$0.046^{+0.050}_{-0.032}$ $0.080^{+0.102}_{-0.057}$	$0.0283^{+0.0064}_{-0.0066}$ $0.0269^{+0.0061}_{-0.0065}$
$e_{\rm avg}$	$0.062^{+0.192}_{-0.039}$ $0.061^{+0.196}_{-0.040}$	$0.0194^{+0.0048}_{-0.0050}$ $0.0194^{+0.0049}_{-0.0047}$	$0.0643^{+0.0092}_{-0.0107}$ $0.0638^{+0.0094}_{-0.0103}$	$0.046^{+0.050}_{-0.032}$ $0.080^{+0.102}_{-0.057}$	$0.0283^{+0.0064}_{-0.0065}$ $0.0269^{+0.0061}_{-0.0065}$
$e\cos\omega$	$0.003^{+0.024}_{-0.023}$ $-0.003^{+0.018}_{-0.024}$	$-0.0000^{+0.0018}_{-0.0019}$ -0.0000 ± 0.0018	0.069 ± 0.013 0.068 ± 0.013	$-0.020^{+0.030}_{-0.063}$ $-0.066^{+0.066}_{-0.108}$	$0.0273^{+0.0064}_{-0.0066}$ $0.0258^{+0.0062}_{-0.0066}$
$e\sin\omega$	$0.023^{+0.021}_{-0.020}$ $0.018^{+0.021}_{-0.018}$	$0.0009^{+0.0026}_{-0.0014}$ $0.0008^{+0.0028}_{-0.0015}$	0.017 ± 0.016 $0.018^{+0.016}_{-0.017}$	$-0.006^{+0.029}_{-0.035}$ $0.002^{+0.051}_{-0.034}$	0.0000 ± 0.0072 0.0036 ± 0.0071
$\omega + M$ (degrees)	$111.56^{+6.90}_{-5.03}$ $112.38^{+8.59}_{-5.05}$	$327.23^{+0.76}_{-0.79}$ $327.18^{+0.75}_{-0.81}$	$361.49^{+5.64}_{-5.70}$ $358.19^{+6.14}_{-6.12}$	$328.00^{+12.66}_{-12.63}$ $324.76^{+12.48}_{-12.70}$	$176.69^{+2.82}_{-2.49}$ $176.32^{+2.62}_{-2.60}$
i (degrees)	$90.58^{+3.57}_{-4.35}$ $90.36^{+3.96}_{-4.66}$	$88.80^{+25.46}_{-23.89}$ $89.73^{+24.49}_{-24.54}$	–	–	–
Ω (degrees)	$353.88^{+21.35}_{-36.65}$ $352.44^{+21.08}_{-122.18}$	0.00 ± 0.00 0.00 ± 0.00	–	–	–

Notes. Time-averaged periods ($P_{\rm avg}$) and eccentricities ($e_{\rm avg}$) are also shown. The other parameters are based on our chosen RV epoch (the first Lick observation). The top value in each cell comes from Case 1 and the bottom value from Case 2.

Table 4. Estimates for the RV zero-point offsets and jitters described in Section 3.2.

Parameter ($m\,s^{-1}$)	Lick	Keck	HET	HJST
$C_{1,X}$	$1.09\pm^{4.77}_{4.97}$	$-32.53\pm^{0.91}_{0.89}$	$1.03\pm^{0.68}_{0.71}$	$-0.24\pm^{0.54}_{0.51}$
	$0.09\pm^{5.23}_{5.30}$	$-32.36\pm^{0.89}_{0.83}$	$0.92\pm^{0.75}_{0.72}$	$0.23\pm^{0.55}_{0.51}$
$C_{2,X}$	$21.34\pm^{3.48}_{3.53}$	-32.91 ± 0.35	–	–
	$21.56\pm^{3.57}_{3.46}$	$-33.13\pm^{0.37}_{0.38}$	–	–
$C_{3,X}$	$-5.82\pm^{0.84}_{0.83}$	–	–	–
	$-6.20\pm^{0.82}_{0.79}$	–	–	–
$C_{4,X}$	$-3.17\pm^{0.94}_{0.87}$	–	–	–
	$-2.86\pm^{0.96}_{0.97}$	–	–	–
$C_{5,X}$	$-6.22\pm^{0.43}_{0.42}$	–	–	–
	-6.49 ± 0.42	–	–	–
$\sigma_{\rm jit,X1}$	$2.37\pm^{3.38}_{1.85}$	$3.46\pm^{0.14}_{0.13}$	$4.66\pm^{0.44}_{0.42}$	$4.85\pm^{0.33}_{0.32}$
	$3.01\pm^{3.98}_{2.37}$	$3.18\pm^{0.15}_{0.14}$	$3.85\pm^{0.49}_{0.46}$	4.66 ± 0.38
$\sigma_{\rm jit,X2}$	$6.06\pm^{0.44}_{0.40}$	–	–	–
	$5.39\pm^{0.48}_{0.47}$	–	–	–
$\sigma_{\rm jit,X3}$	$6.75\pm^{0.29}_{0.26}$	–	–	–
	$6.35\pm^{0.32}_{0.31}$	–	–	–

Notes. The top value in each cell comes from Case 1 and the bottom value from Case 2.

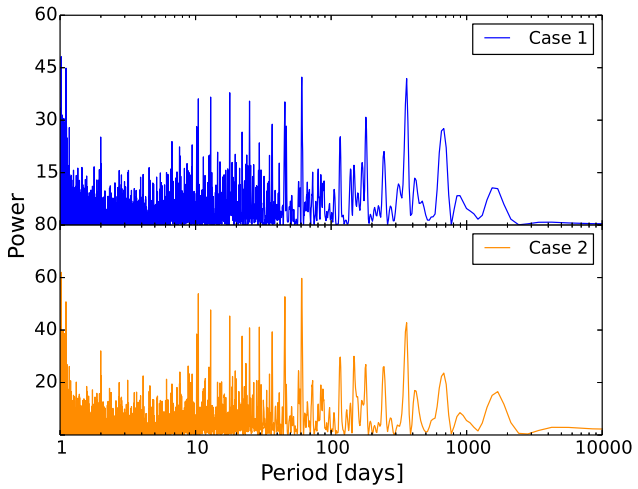

Figure 1. The periodogram of RV residuals for Cases 1 (top, blue) and 2 (bottom, orange). We do not probe the sub-day regime as we do not expect to find planets in addition to 'e' in this period domain.

the presence of the other planets may maintain an excited orbit (Dawson & Fabrycky 2010).

We perform transit timing variation (TTV) simulations to address how significantly the outer four planets affect the orbit of planet 'e' (Ford & Holman 2007; Veras, Ford & Payne 2011). The TTV amplitude, i.e. the maximum about of time which the orbit of 'e' deviated from a linear ephemeris, was of the order of seconds, much smaller than the observing cadence for binned observations with *Spitzer* or *MOST*. Therefore, we expect its transit times to be very nearly periodic.

Because we allowed planet 'e' to have a different i and Ω than the outer planets, we can attempt to constrain the mutual inclination, $i_{\rm mut}$, with the rest of the planets. Before we impose the constraint of dynamical instability, more than half of our models had planet 'e' in a retrograde orbit. Because 'e' was found to be dynamically decoupled from the rest of the planets, these models are indistinguishable on the observing baseline from that of a prograde orbit. By integrating these systems for 10^5 yr, we find that most models with large $i_{\rm mut}$ are dynamically unstable (Fig. 2, left). The outcome of the instability is the innermost planet being accreted by the host star. The time until accretion is rapid ($<10^5$ yr) for all mutual inclinations that result in instability. The instability is typically even more rapid ($<10^3$ yr), with the exception of $i_{\rm mut} \sim 125^\circ$. Note that we find no indication of instability for orbits with $i_{\rm mut} > 125^\circ$. We do not find any strong correlations between planet e's stability and any other parameters. Therefore, we obtain a new set of 10 000 posterior samples that do not include systems with $60^\circ < i_{\rm mut} < 125^\circ$. In Fig. 2, there are overlapping stable and unstable solutions near 125°. These solutions are unstable on longer time-scales (to be discussed in Section 4.5), so we consider 125° to be a conservative cutoff. It is worth noting that when we include the effects of relativistic precession on planet 'e', most of these retrograde orbits become unstable. We find the timescale for this relativistic precession is comparable to that of the secular interactions.

In the right-hand panel of Fig. 2, we show distributions of planet mass for Cases 1 and 2. The additional RVs plus the self-consistent dynamical model of the system provide an improved constraint on the mass and density of planet 'e'. The median value is roughly 2σ lower than the Winn et al. (2011) value and 1σ lower than the Endl et al. (2012) value. The uncertainty in mass is nearly $\sim$3 per cent in both cases. Using the Winn et al. (2011) planet-to-star radius ratio, we constrain the density of 'e' to $5.44\pm^{1.29}_{0.98}$ and $5.51\pm^{1.32}_{1.00}$ g cm^{-3} for Cases 1 and 2, respectively.

We do not include the effects of tidal dissipation on the 55 Cancri system, as the tidal dissipation rate is highly uncertain. Bolmont et al. (2013) find tidal dissipation time-scales for $>10^5$ yr, even for very high tidal efficiencies. Therefore, tides will have a negligible effect on the system over the time-scale of observations being analysed. They find tides affect the orbital evolution on time-scales of $\sim 3 \times 10^4$ yr. For most mutual inclinations that result in instability,

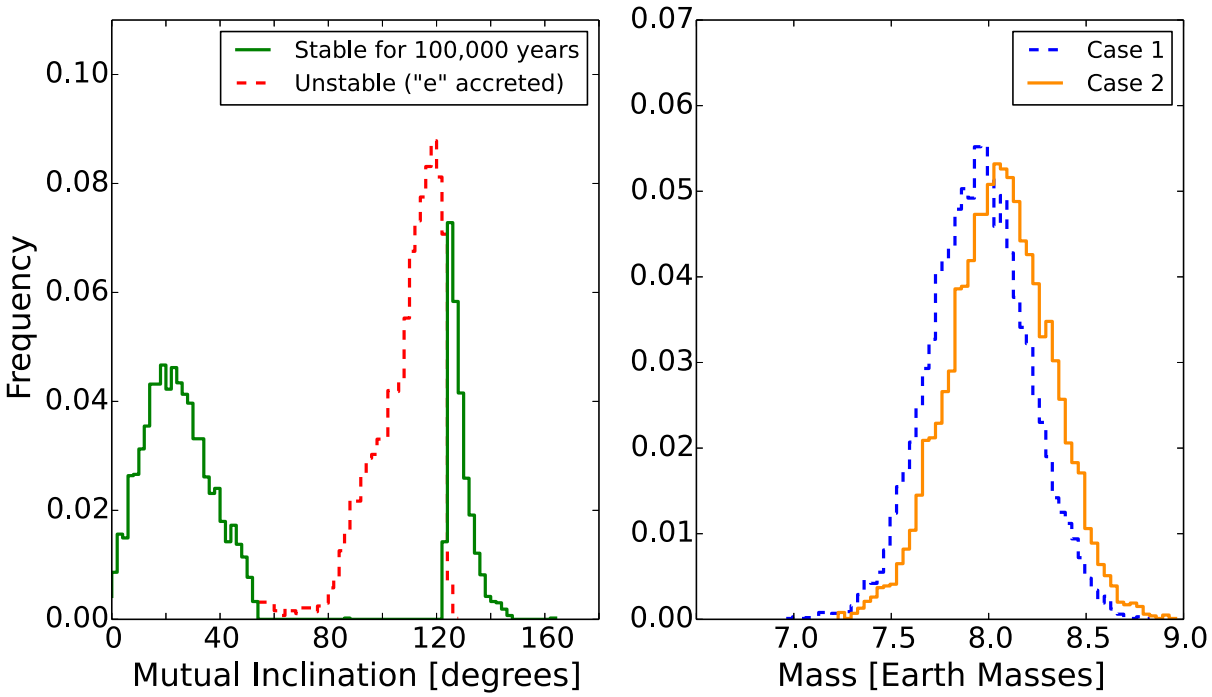

Figure 2. Properties of the inner-most planet, 'e'. Left: two distributions of the mutual inclination between planet 'e' and the outer four (coplanar) planets for Case 2. In 10 000 dynamical simulations, 5056 systems had the innermost planet spiral into 55 Cancri A within 10^5 yr (normalized distribution in red/dashed). The remaining systems (normalized distribution in green/solid) showed no signs of instability, defined in Section 4.3. Right: distribution of planet mass for Case 1 (blue, dashed) and Case 2 (orange, solid). Mass estimates with respect to previous results are listed as follows: 8.63 ± 0.35 (Winn et al. 2011), 8.37 ± 0.38 (Endl et al. 2012), 7.99 ± 0.25 (Case 1), 8.09 ± 0.26 $M_\oplus$ (Case 2).

the time-scale to instability is significantly shorter than the predicted tidal evolution time-scale. Our measurement of the eccentricity for planet 'e' is inconsistent with significantly faster tidal dissipation.

Our orbital parameter estimates listed in Table 3 represent a significant improvement on those of Dawson & Fabrycky (2010) and Endl et al. (2012). We find the eccentricity of planet 'e' ($e_e = 0.028 \pm^{0.022}_{0.019}$) is significantly less than the estimate from Dawson & Fabrycky (2010) ($e_e = 0.17$). Thus, the current eccentricity places a much weaker constraint on the tidal efficiency than the previous analysis of Bolmont et al. (2013) that assumed initial conditions from Dawson & Fabrycky (2010). Bolmont et al. (2013) also found the initial conditions derived from Endl et al. (2012) to be dynamically unstable, and thus not a realistic model. Furthermore, since Endl et al. (2012) assumed a circular orbit for planet 'e', their orbital model is of limited value for exploring the tidal evolution of the system. Nevertheless, many of the qualitative conclusions from Bolmont et al. (2013) about the long-term eccentricity evolution of the system are likely applicable, since their measurements of the eccentricities for planets 'b' and 'c' are similar to those of our more detailed modelling. Using the Endl et al. (2012) initial conditions, Bolmont et al. (2013) predict e_e approaches an equilibrium where the eccentricity periodically varies from a nearly circular configuration to maximum eccentricity of $\sim 5 \times 10^{-4}$ to 0.013.

4.2 The near-resonant pair, 55 Cancri b and c

In Fig. 3, we show 68.3 and 95.4 per cent credible interval contours in P_b and P_c space for Case 2. Most previous analyses for 55 Cancri assumed independent Keplerian orbits, but Fig. 3 demonstrates the importance of N-body effects during the $\sim$23 yr of observations. Our N-body analysis adopts a Jacobi coordinate parametrization based

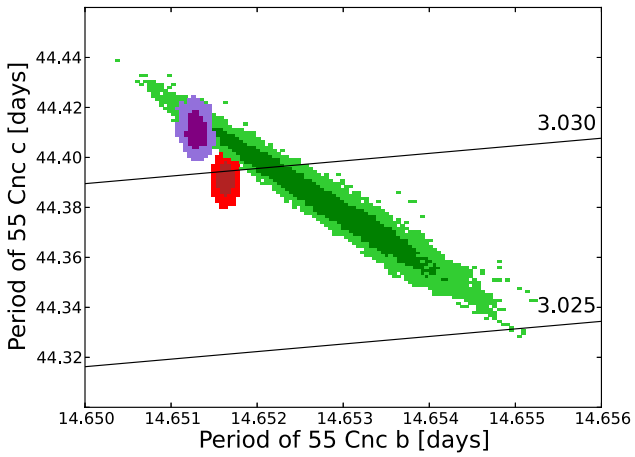

Figure 3. Estimates of the period ratio of the 'b' and 'c' pair for Case 2. Two lines of constant period ratio (3.025, 3.030) are shown for reference. We draw 10 000 independent samples from a Keplerian MCMC (red). Choosing the RV epoch to be the first Lick observation, we draw 10 000 samples that are also vetted for stability (see Fig. 2) from a RUN DMC (green) analysis. For reasons stated in the text (Section 4.2), we compute time-averaged orbital period estimates of the raw RUN DMC solutions over the 10^5 yr integration (purple). 1σ and 2σ credible contours are constructed, shown as the darker and lighter colour, respectively.

on an epoch corresponding to the first Lick observation in 1989 February. Using MERCURY, we extend the integration for 10^5 yr on a 10 000 dynamically 'stable' models described in Section 4.1 and find the maximum variability in the semimajor axes of planets 'b' and 'c' is comparable to or even exceeds the 68.3 per cent credible intervals of the respective semimajor axis distributions. The epoch

for initial conditions happened to be around this maximum, so our time averaged estimates for P_b and P_c are not centred on the contour of the raw RUN DMC orbital periods. The median values of the Keplerian and *N*-body solutions are separated by $\sim 6\times$ the standard deviation of the joint Keplerian distribution in P_b–P_c space.

The three resonant angles associated with the 3:1 MMR were circulating for nearly all of our models, so these two planets are not in a mean-motion resonance. This is consistent with the findings of Fischer et al. (2008), and from our large sample size, we can conclude that this result robust.

Nevertheless, they are near enough to the 3:1 MMR that they can interact significantly and exhibit interesting interactions. In particular, they might develop a secular lock, a configuration where both periastrons precess at the same time-averaged rate, and the gravitational kicks from frequent conjunctions cause libration of the angle between their pericentre directions. We consider a subset of 10 000 models from Cases 1 and 2 and track the orbital evolution for 10^5 yr using MERCURY. We compute the rms of the angle $\varpi_b - \varpi_c$, using six different phase domains for the angle (0 to 2π, $-5\pi/3$ to $1\pi/3$, $-4\pi/3$ to $2\pi/3$, $-\pi$ to π, $-2\pi/3$ to $4\pi/3$, $-\pi/3$ to $5\pi/3$). We find the smallest rms value and report the value centred on the domain with the smallest rms value. The vast majority of cases were centred about π (180°). While many of these are librating, some systems that are circulating but evolve more slowly when the secular angle is near π might also be classified as librating. Additionally, the short-term interactions with the other planets can cause the long-term librating behaviour of 'b' and 'c' to occasionally circulate.

We considered multiple methods for estimating the libration amplitude for each of these models. The naive approach would be to simply compute half of the peak-to-peak variation. However, the secular interactions between planets 'b' and 'c' sometimes pushed them towards very low eccentricity. For nearly circular orbits, short-term perturbations can cause $\varpi_b - \varpi_c$ to take on extreme values even for systems undergoing secular libration. Thus, the peak-to-peak method overestimates the libration amplitude for many systems. This was remedied by applying an eccentricity cutoff to filter out values of $\varpi_b - \varpi_c$ when e_b or $e_c < 0.001$. We found the shape of the resulting libration amplitude distribution was strongly dependent on our chosen cutoff value. In light of this, we tried other metrics more robust to outliers, such as the rms and median absolute deviation (MAD). For a system undergoing small amplitude, sinusoidal libration, rms$\times\sqrt{2}$ and MAD$\times\sqrt{2}$ are excellent approximations for the libration amplitude.

We found a wide range in $\varpi_b - \varpi_c$ behaviour, so there was not one metric that could accurately differentiate libration from circulation. Instead, we compute the rms and peak-to-peak variation of the secular angle including only values where both eccentricities exceed 0.001. Fig. 4 shows a scatter plot of the rms and peak-to-peak variation for 10 000 'stable' models from Section 4.1 for each case. Based on visual inspection, we find that small amplitude librations typically have rms($\varpi_b - \varpi_c$) < 67° (corresponding to a libration amplitude less than 90°) and a peak-to-peak variation <260°. The median libration amplitude of this subset of models is $51^\circ \pm^{6^\circ}_{10^\circ}$ (68.3 per cent credible interval) for both Cases 1 and 2. Circulating systems typically have rms > 70.0 and peak-to-peak variation >340°, but many of these were 'nodding', meaning that $\varpi_b - \varpi_c$ exchanges between cycles of libration and circulation (Ketchum, Adams & Bloch 2013). Those that do not meet either of these aforementioned criteria fall into the 'ambiguous' category. By inspection, many of the ambiguous systems have large libration amplitudes with short-term perturbations, while others show long-term nodding. Under our empirically derived definitions for libration and

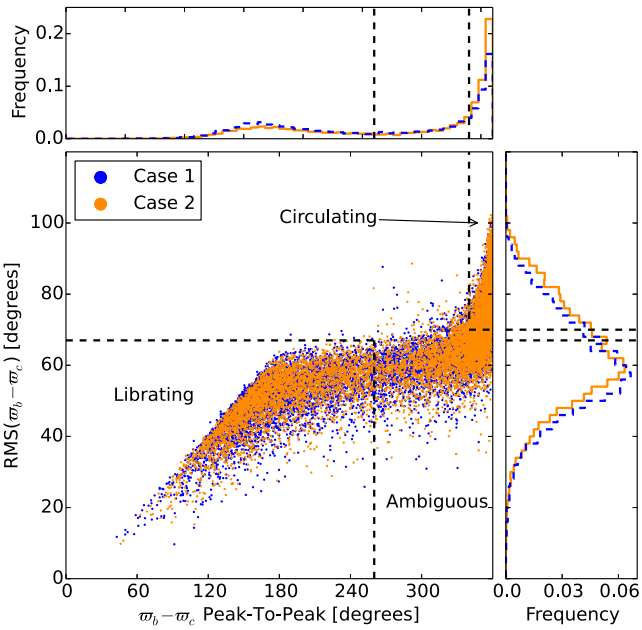

Figure 4. The secular behaviour of 10 000 model systems for Case 1 (blue, dashed) and Case 2 (orange, solid) as discussed in Section 4.2. The horizontal axis shows the peak-to-peak variation in secular angle ($\varpi_b - \varpi_c$) only when the eccentricity of either planet was greater than 0.001. The vertical axis shows the rms of the secular angle variation. Librating systems typically had rms <67° and peak-to-peak variation <260°. Circulating systems typically had rms >70° and peak-to-peak variation >340°. Those that did not fall into either of these categories displayed an array of secular behaviour, ranging from large amplitude libration with short term variations to long-term 'nodding' (Ketchum et al. 2013).

circulation, we find the fraction of stable systems undergoing the following types of secular behaviour: librating, 44.6 per cent (36.5 per cent); circulating/nodding, 20.3 per cent (28.2 per cent); and ambiguous, 35.1 per cent (35.3 per cent) for Case 1 (Case 2).

Case 2 favours a larger eccentricity value for planet 'f' than Case 1. This could suggest that the closer periastron passages of 'f' in Case 2 disrupts the secular lock of the near-resonant pair, causing a greater fraction of modelled systems to circulate.

4.3 The habitable zone planet, 55 Cancri f

When the three-planet model of 55 Cancri was announced by Marcy et al. (2002), there was a noticeably wide semimajor axis gap between planets 'c' and 'd'. An unseen planet could reside in this dynamically stable gap, possibly one massive enough to induce a clear RV signal (Raymond et al. 2008). Fischer et al. (2008) announced the fifth planet, 'f', a sub-Jovian mass planet on a Venus-like orbit, residing in the classical habitable zone. Because it induces the weakest RV signal of all the 55 Cancri planets, its eccentricity is not well constrained; in Case 1, its eccentricity is consistent with circular, but in Case 2, it has a substantial range in eccentricity with a median of ∼0.1. In the latter case, the stellar flux it receives over time could vary substantially.

4.4 The Jupiter analogue, 55 Cancri d

In terms of its measured period and eccentricity, planet 'd' is the closest Jupiter analogue to date. The Endl et al. (2012) estimates are $P_d = 4909 \pm 30$ d and $e_d = 0.02 \pm 0.008$, compared to that of Jupiter: $P_J \approx 4333$ d and $e_J \approx 0.049$. Our posterior samples not only

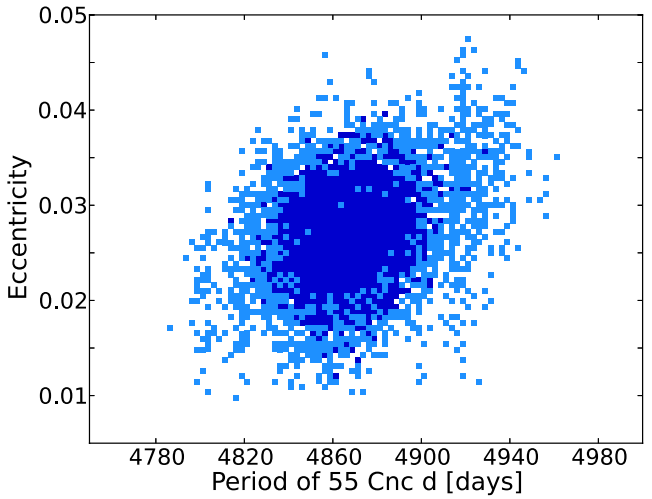

Figure 5. Marginal posterior density for time-averaged period and time-averaged eccentricity of 55 Cancri 'd', based on Case 2.

improve the parameter uncertainties, but also nudge the estimated period and eccentricity closer to that of Jupiter ($P_{\rm d} \approx 4867$ d and $e_{\rm d} \approx 0.0269$). Although 'd' has yet to undergo two full period cycles, we are able to infer small but measurable eccentricity (Fig. 5).

4.5 Long-term stability

We tested the long-term stability of the system, excluding the wide binary companion. We modified MERCURY such that if any planet's semimajor axis changes by more than 50 per cent of its original value ($|[a_{\rm final} - a_{\rm initial}]/a_{\rm initial}| > 0.5$), then the simulation stops and is tagged as being unstable. First, we evolved 1000 five-planet models for 10^6 yr, and identified 9.4 per cent as unstable within $60^\circ < i_{\rm mut} < 125^\circ$. The stability was most sensitive to the mutual inclination between the orbital plane of planet 'e' and the common orbital plane of the remaining planets on this longer time-scale. Over 90 per cent of the unstable solutions were those where $i_{\rm mut} \sim 125^\circ$, and planet 'e' was accreted by its host star. However, we still found stable solutions with planet 'e' orbiting retrograde. Thus, dynamical stability provides constraints on $i_{\rm mut}$, as described in Section 4.1. For systems with $i_{\rm mut} < 60^\circ$, the inner planet was dynamically decoupled from the outer four planets.

Next, we evolved 1000 four-planet models (excluding the innermost planet) for 10^8 yr. None of the 1000 model systems tested were identified as unstable. Thus, the extensive RV observations now provide such tight constraints on the planet masses and orbital parameters that essentially all allowed nearly coplanar solutions are dynamically stable.

Prior to our final analysis, we preformed several preliminary analyses based on a different set of observations [fewer RV measurements, Lick velocities from Fischer et al. (2008) rather than improved reduction in 2014]. The posterior samples included some models with the eccentricity of planet 'f' exceeding 0.3. For many of these sets of initial conditions, systems would become unstable, recognized by a significant change in semimajor axis of planet 'c' or 'f' on a time-scale of $\sim 10^6$–10^8 yr. We conclude that the tighter constraint on the eccentricity of planet 'f' based on our final analysis was responsible for ensuring that none of the 1000 model systems from our final analysis showed signs of dynamical instability.

5 DISCUSSION

We report the first self-consistent Bayesian analysis of the 55 Cancri system that uses *N*-body integrations to account for the planets' mutual gravitational interactions. By combining a rigorous statistical analysis, dynamical model and improved observational constraints, we obtain the first set of five-planet models that are dynamically stable. We considered two extreme cases where the high-cadence, unbinned RV measurements were treated as independent (Case 1) or perfectly correlated (Case 2). In both cases, the RV residuals show no immediately convincing signals due to an additional sixth planet.

Informative priors based on precise photometry from *MOST* (Winn et al. 2011) drastically narrow the possible orbital inclination range of planet 'e'. The planet–planet interactions amongst the remaining planets provide a loose inclination constraint just based on the RVs. Combining all this information yields a mutual inclination estimate. Under the assumption of relatively short-term dynamical stability (10^5 yr), we find planet 'e' cannot be highly misaligned with the outer four planets. However, there are some stable configurations where 'e' orbits retrograde as long as the mutual inclination is nearly retrograde ($125 < i \leq 180^\circ$). To be consistent with our photometric knowledge, we utilize the *MOST* planet-to-star radius ratio measurement to obtain a density estimate of $5.44 \pm^{1.29}_{0.98}$ and $5.51 \pm^{1.32}_{1.00}$ g cm^{-3} for Cases 1 and 2, respectively. Assuming the derived mass for 'e' is insensitive to our priors on the central transit time, transit duration, and ingress duration, the radius ratio estimate from Gillon et al. (2012) gives alternative densities of $4.28 \pm^{0.65}_{0.55}$ and $4.34 \pm^{0.66}_{0.55}$ g cm^{-3} for Cases 1 and 2, respectively.

We find that planets 'b' and 'c' are not in the 3:1 MMR, as all of the associated resonant angles are circulating. We also find between a 36 and 45 per cent chance for the pericentre directions of planets 'b' and 'c' to exhibit secular lock with $\varpi_{\rm b} - \varpi_{\rm c}$ librating about 180°. The behaviour of this angle is only weakly constrained by the present observations, with a substantial fraction of solutions resulting in circulating or nodding of the secular angle.

Using the latest RV data sets, we find the vast majority of, if not all, models of the outer-four planets are long-term stable. We expect that tidal effects and gravitational perturbations due to planet 'e' are negligible over these time-scales.

Despite the large dimensionality, short integration timestep, and a lengthy mixing time, we have obtained a set of effectively independent posterior samples available to the exoplanet community for more detailed future studies. The improved mass and density estimates for 'e' will certainly provide new insight to the interior bulk composition. If it turns out that planet 'b' has an extended atmosphere that grazes its host star (Ehrenreich et al. 2012), our updated orbital period and mass estimates will be valuable in modelling the planet's atmosphere and potentially providing a sharper orbital inclination estimate. Astrometric observations of 55 Cancri A with the *Hubble Space Telescope* (*HST*) traced out a small arc, presumably dominated by orbit of planet 'd' (McGrath et al. 2003). In combination with RVs, the orbital inclination of the outermost planet was estimated to be $53^\circ \pm 6.^\circ 8$ (McArthur et al. 2004), but this relies on an accurate assessment of d's orbital period, which has changed significantly since then. We recommend a re-analysis of the *HST* data with the new orbital model and incorporating the M dwarf companion to improve the astrometric constrain on its orbital inclination.

For the advancement of the exoplanet field in general, we are releasing the posterior samples from this analysis and encourage others to do the same for future announcements or updates to

individual planetary systems. Posterior samples for Case 1 and Case 2 are available as Supporting Information with the online version of the article. In particular, it has now become practical to use hierarchical Bayesian models to infer properties of the exoplanet population. Understanding the nature behind the uncertainties in orbital period, mass, eccentricity, etc. beyond the 1σ values is crucial for such a study.

ACKNOWLEDGEMENTS

We would like to thank our referee Sean Raymond for his helpful comments on the manuscript. B.E.N. thanks Eric Feigelson and Brad Hansen for insightful discussions of that helped strengthen the paper. We thank Geoff Marcy and the entire of the California Planet Survey team for their long-term commitment to high-precision RVs for the 55 Cancri system. We also thank Stan Dermott for his contribution to this project. This research was supported by NASA Origins of Solar Systems grant NNX09AB35G and NASA Applied Information Systems Research Programme grant NNX09AM41G. The authors acknowledge the University of Florida High Performance Computing Center for providing computational resources and support that have contributed to the results reported within this paper. The Center for Exoplanets and Habitable Worlds is supported by the Pennsylvania State University, the Eberly College of Science, and the Pennsylvania Space Grant Consortium. We extend special thanks to those of Hawai'ian ancestry on whose sacred mountain of Mauna Kea we are privileged to be guests. Without their generous hospitality, the Keck observations presented herein would not have been possible.

REFERENCES

Baluev R. V., 2013, Astron. Comput., 3, 50
Barnes R., Greenberg R., 2007, ApJ, 665, L67
Bolmont E., Selsis F., Raymond S. N., Leconte J., Hersant F., Maurin A.-S., Pericaud J., 2013, A&A, 556, A17
Butler R. P., Marcy G. W., Williams E., McCarthy C., Dosanjh P., Vogt S. S., 1996, PASP, 108, 500
Butler R. P., Marcy G. W., Williams E., Hauser H., Shirts P., 1997, ApJ, 474, L115
Chambers J. E., 1999, MNRAS, 304, 793
Dawson R. I., Fabrycky D. C., 2010, ApJ, 722, 937
Demarque P., Woo J.-H., Kim Y.-C., Yi S. K., 2004, ApJS, 155, 667
Demory B.-O. et al., 2011, A&A, 533, A114
Demory B.-O., Gillon M., Seager S., Benneke B., Deming D., Jackson B., 2012, ApJ, 751, L28
Dindar S., Ford E. B., Juric M., Yeo Y. I., Gao J., Boley A. C., Nelson B., Peters J., 2013, New Astron., 23, 6
Dragomir D., Matthews J. M., Winn J. N., Rowe J. F., MOST Science Team, 2013, preprint (arXiv:1302.3321)
Ehrenreich D. et al., 2012, A&A, 547, A18
Endl M. et al., 2012, ApJ, 759, 19
Fischer D. A. et al., 2008, ApJ, 675, 790
Fischer D. A., Marcy G. W., Spronck J. F. P., 2014, ApJS, 210, 5
Ford E. B., 2006, ApJ, 642, 505
Ford E. B., Holman M. J., 2007, ApJ, 664, L51
Gillon M. et al., 2012, A&A, 539, A28
Ji J., Kinoshita H., Liu L., Li G., 2003, ApJ, 585, L139
Kaib N. A., Raymond S. N., Duncan M. J., 2011, ApJ, 742, L24
Ketchum J. A., Adams F. C., Bloch A. M., 2013, ApJ, 762, 71
Kley W., Peitz J., Bryden G., 2004, A&A, 414, 735
Kokubo E., Yoshinaga K., Makino J., 1998, MNRAS, 297, 1067
McArthur B. E. et al., 2004, ApJ, 614, L81
McGrath M. A. et al., 2003, in Deming D., Seager S., eds, ASP Conf. Ser. Vol. 294, Scientific Frontiers in Research on Extrasolar Planets. Astron. Soc. Pac., San Francisco, p. 145
Madhusudhan N., Lee K. K. M., Mousis O., 2012, ApJ, 759, L40
Marcy G. W., Butler R. P., 1992, PASP, 104, 270
Marcy G. W., Butler R. P., Fischer D. A., Laughlin G., Vogt S. S., Henry G. W., Pourbaix D., 2002, ApJ, 581, 1375
Mugrauer M., Neuhäuser R., Mazeh T., Guenther E., Fernández M., Broeg C., 2006, Astron. Nachr., 327, 321
Nelson B. E., Ford E. B., Payne M. J., 2014, ApJS, 210, 11
Raymond S. N., Barnes R., Gorelick N., 2008, ApJ, 689, 478
Rivera E. J., Laughlin G., Butler R. P., Vogt S. S., Haghighipour N., Meschiari S., 2010, ApJ, 719, 890
Tan X., Payne M. J., Lee M. H., Ford E. B., Howard A. W., Johnson J. A., Marcy G. W., Wright J. T., 2013, ApJ, 777, 101
ter Braak C. J. F., 2006, Stat. Comput., 16, 239
Teske J. K., Cunha K., Schuler S. C., Griffith C. A., Smith V. V., 2013, ApJ, 778, 132
Valenti J. A., Butler R. P., Marcy G. W., 1995, PASP, 107, 966
Van Laerhoven C., Greenberg R., 2012, Celest. Mech. Dyn. Astron., 113, 215
Veras D., Ford E. B., Payne M. J., 2011, ApJ, 727, 74
Vogt S. S. et al., 1994, in Crawford D. L., Craine E. R., eds, Proc. SPIE Conf. Ser., Vol. 2198, Instrumentation in Astronomy VIII. SPIE, Bellingham, p. 362
von Braun K. et al., 2011, ApJ, 740, 49
Winn J. N. et al., 2011, ApJ, 737, L18
Zhou L.-Y., Lehto H. J., Sun Y.-S., Zheng J.-Q., 2004, MNRAS, 350, 1495

SUPPORTING INFORMATION

Additional Supporting Information may be found in the online version of this article:

Table 1. Keck HIRES Radial Velocities for 55 Cancri. (http://mnras.oxfordjournals.org/lookup/suppl/doi:10.1093/mnras/stu450/-/DC1).

Please note: Oxford University Press are not responsible for the content or functionality of any supporting materials supplied by the authors. Any queries (other than missing material) should be directed to the corresponding author for the article.

This paper has been typeset from a TEX/LATEX file prepared by the author.